New Journal of Physics
The open access journal at the forefront of physics

Deutsche Physikalische Gesellschaft DPG
IOP Institute of Physics

Published in partnership with: Deutsche Physikalische Gesellschaft and the Institute of Physics

OPEN ACCESS

RECEIVED
29 July 2015

REVISED
3 October 2015

ACCEPTED FOR PUBLICATION
10 November 2015

PUBLISHED
4 December 2015

PAPER

Electrical conduction of ion tracks in tetrahedral amorphous carbon: temperature, field and doping dependence and comparison with matrix data

J Krauser[1], H-G Gehrke[2,6], H Hofsäss[2], J Amani[2], C Trautmann[3,4] and A Weidinger[5]

[1] Harz University of Applied Sciences, D-38855 Wernigerode, Germany
[2] II. Institute of Physics, University of Göttingen, D-37077 Göttingen, Germany
[3] Helmholtzzentrum für Schwerionenforschung, D-64291 Darmstadt, Germany
[4] Technische Universität Darmstadt, D-64287 Darmstadt, Germany
[5] Helmholtz-Zentrum Berlin, D-14109 Berlin, Germany
[6] Present address: Forschungszentrum Jülich GmbH, D-52428 Jülich, Germany

E-mail: hhofsae@uni-goettingen.de

Keywords: conducting ion tracks, tetrahedral amorphous carbon, conduction mechanism

Abstract

This paper gives an extended overview of the electrical properties of ion tracks in hydrogen-free tetrahedral amorphous carbon (ta-C) with a sp^3 bond fraction of about 80%. The films were grown by mass selected ion beam deposition of 100 eV $^{12}C^+$ ions. The ion tracks are generated by irradiation of ta-C films with uranium ions of 1 GeV kinetic energy. Along the ion path a conversion from diamond-like (sp^3) carbon to graphite-like (sp^2) carbon takes place. Topography and current measurements of individual ion tracks were performed by atomic force microscopy at ambient temperature. The temperature dependence of the electric conductivity was studied between 15 and 390 K by means of 0.28 mm^2 large contact pads averaging over about 10^7 tracks. For each sample and at each temperature the conductivity as a function of the applied electrical field (non-ohmic behaviour) was measured separately and the data were extrapolated to field zero. In this way, the zero-field conductivity was determined independent from the field dependence. In spite of large differences in the absolute values, the temperature dependence of the zero-field conductivities is found to be very similar in shape for all samples. The conductivities follow a $T^{-1/4}$ law up to temperatures slightly below room temperature. At higher temperatures a transport mechanism based on over-barrier hopping dominates with an activation energy of about 220 meV for tracks and 260 meV for the ta-C matrix. The field dependence measurements show that the deviation of the I–V characteristics from ohmic behaviour decreases with increasing zero-field conductivity. We also tested Cu-doped ta-C samples and found that they conduct significantly better than pure ta-C. However, the doping also increases the zero-field conductivity resulting in a weaker contrast between the track and matrix. The data are interpreted within the so-called 'barrier model' where the electrons are assumed to move fairly freely in well-conducting sp^2 regions but encounter barriers in track sections consisting of more sp^3-like bonds.

1. Introduction

Under swift heavy ion irradiation, amorphous carbon materials undergo structural changes resulting in a modification of the sp^3/sp^2 ratio along the ion trajectories. In diamond-like tetrahedral amorphous carbon (ta-C) a change to a more graphitic form has been found (Waiblinger *et al* 1999). This effect can be used to selectively modify the electrical properties on a nanometer scale since the resulting tracks constitute electrically conducting nanowires embedded in the insulating ta-C matrix. The tracks have an extremely small diameter (~8 nm) and a length up to several μm, suggesting possible use in future nano-electronic devices (Weidinger 2004, Krauser *et al* 2008, Gehrke *et al* 2010).

Earlier experimental work focussed mainly on the improvement of the track conductivity by changing experimental conditions (Zollondz *et al* 2006, Nix *et al* 2007, Krauser *et al* 2011, 2013). The most important parameter for high conductance is the specific energy loss of the ions. Only very heavy ions with energies of several 100 MeV create well-conducting tracks. Controlled doping of the ta-C matrix yielded also some improvement of the tracks (Nix 2010, Krauser *et al* 2012). The highest track conductivity (10^3 S m^{-1}) measured so far was obtained in a 1 at.% Fe-doped ta-C film irradiated with C_{60} cluster ions (Krauser *et al* 2013). Among the monoatomic projectiles 1 GeV uranium ions are the most suited particles due to their high energy loss in ta-C of $dE/dx \sim 40$ keV nm^{-1}. This ion beam was also used in the present study.

An important aspect is the behaviour of the conducting ion tracks under an applied electrical field. In most cases (see references in the preceding chapter) a bending of the current-voltage characteristics, i.e., a deviation from Ohm's law was observed. A tendency to less bending shows up for the better conducting tracks; the current–voltage characteristics for ta-C samples irradiated with C_{60} and for some doped samples irradiated with uranium ions are linear at room temperature. The bending effect has not yet been studied systematically and is a major point in the present investigation.

These earlier experiments, summarized in (Krauser and Weidinger 2012), were mainly limited to room temperature except for a few low temperature measurements (Schwen 2007, Gehrke 2008, Nix 2010). The main progress in the present work is the extension of this investigations to low temperatures down to 15 K. A complete set of temperature- and field-dependence data is presented together with a detailed discussion and interpretation of the results. The data were obtained to a large extend within the framework of the doctoral thesis of Gehrke (2013).

In the past, the temperature dependence was usually measured at a fixed applied voltage. Due to the bending of the *I–V* characteristics and the variation of the bending with temperature, one obtains a mixture of temperature and field dependence, which makes the analysis difficult. In the present study we separated these two effects by recording at each temperature a full *I–V* curve and fitting these curves with a theoretical function. The extrapolation to $V = 0$ V yields the zero-field conductivity and the bending of the curves reflects the field dependence. Both, the zero-field conductivity and the bending parameter are plotted and analysed as a function of temperature.

Earlier investigations using Cu-doped ta-C samples indicated that a slight admixture of Cu might improve the performance of ion tracks (Krauser *et al* 2012, 2013), while other doping elements were less promising. However, the optimum amount of doping remained unclear. In order to better evaluate the advantages and disadvantages of doping, we performed new measurements with different Cu concentrations and compare the effect of doping on the electrical conductivity of tracks with that on the matrix. It should be noted that doping is used here in the general sense of adding a small amount of foreign atoms to the material. It does not imply that the added atoms are electrically active.

For the interpretation of the data the so-called 'barrier model' was developed. The main assumption is that barriers consisting of a few sp^3-like bonds interrupt the fairly free movement of electrons in sp^2-like regions. The formulas used in the analysis are similar to those used in literature but the interpretation of the fit parameters is quite different.

2. Experimental

The acronym ta-C is nowadays used for a variety of carbon materials grown by different industrial scale plasma-enhanced PVD or CVD processes or by vacuum arc deposition (VDI 2840 2005, Neuville 2014). Depending on the growth process and the application, the properties of ta-C may differ significantly, in particular the hardness, the sp^3 bond fraction, the resistivity and the optical band gap may be reduced in so-called degraded, more graphitic ta-C (for a general review on ta-C and DLC materials see Robertson 2002, Neuville 2014).

For our studies we use ta-C films grown by mass selected ion beam deposition (MSIBD) of 100 eV $^{12}C^+$ ions on Si substrates kept at room temperature (Hofsäss *et al* 1993, Ronning 2003), a non-industrial deposition process which produces practically hydrogen-free amorphous carbon films with a C-sp^3 bond fraction of about 80%. Therefore, the ta-C films used in our work can be considered as the most diamond-like, hard ta-C films.

The properties of MSIBD grown ta-C films were previously investigated also by other groups such as Lifshitz *et al* (1994). Films grown with ion energies around 100 eV exhibit a very smooth surface often with rms roughness well below 1 nm (Lifshitz 1999). The ultrasmoothness of such ta-C films was recently investigated theoretically by Moseler *et al* (2005). The sp^3 content in MSIBD grown ta-C films was determined by Kulik *et al* using inelastic and elastic electron scattering carried out in a transmission electron microscope (Kulik *et al* 1995). In this work, the sp^3 content was derived from an analysis of the carbon K-edge spectra, the plasmon energies and the reduced density function (radial distribution function). For ta-C films deposited at room temperature, a sp^3 content of 80% was found for C^+ ion energies between 50 and 600 eV. For a deposition energy around

100 eV the films exhibit the most diamond-like properties, regarding average bond length (1.53 Å), average bond angle (111°) and plasmon energy (30–31 eV).

The properties of our MSIBD ta-C films were characterized by electron energy loss spectroscopy using XPS or Auger electron spectroscopy, Raman spectroscopy, atomic force microscopy (AFM), Rutherford backscattering, nuclear reaction analysis (NRA), Vickers indentation measurements, ultraviolet photoelectron spectroscopy (UPS) valence band spectroscopy and electrical measurements.

The Raman spectra of these films are an indication for amorphous carbon because they show a broad distribution of the Raman intensity between 1400 and 1700 cm^{-1} and no diamond-band or D- and G-bands of graphite (Hofsäss *et al* 1993). The as deposited ta-C films are very smooth with an rms roughness below 0.8 nm (Hofsäss *et al* 2009) often even 0.2 nm (Takahiro *et al* 2007). The films exhibit a high resistivity of up to 10^{10} Ω cm, which decreases upon doping with N or B atoms (Ronning and Hofsäss 1995).

The Vickers hardness of the films is about 4500 kg mm^{-2} (Hofsäss *et al* 1993), which is in agreement with results of Koskinen for ion beam deposited ta-C films (Koskinen 1988). The sp^3 content of our films was determined from plasmon energies and is about 80%, corresponding to plasmon energies of 31 eV (Ronning *et al* 1997, Hofsäss *et al* 1998). Our MSIBD ta-C films were also analysed by high resolution TEM revealing a plasmon energy of 30.8 eV for deposition at 50 eV and 31.8 eV for deposition at 100 eV (Christiansen *et al* 1998). Furthermore, there is no indication in the C K-edge spectra of the narrow peak at 285 eV typical for sp^2 carbon. These values are in good agreement with results of several other groups obtained for ta-C films grown by ion beam deposition or filtered vacuum arc deposition with carbon ion energies around 100 eV (Hofsäss *et al* 1998).

With UPS valence band spectroscopy it is possible to distinguish between π and σ bond states. For undoped ta-C films we find an intense peak related to σ bonds and a weak peak related to π bonds, from which a sp^2 bond fraction of 17 $\pm$ 5% was calculated (Ronning *et al* 1997).

The hydrogen content of various films was measured by NRA using the H (^{15}N, $\alpha\gamma$)^{12}C resonance reaction. For our MSIBD grown films the H content is far below 0.1 at.%, whereas films grown by filtered arc deposition contain about 1 at.% hydrogen (Krauser *et al* 2003). Possible metal contaminations due to sputtering from the stainless steel ion optics components of the ion deceleration unit was determined to be less than 10 ppm (Hofsäss *et al* 1993).

Copper doped ta-C films were prepared by our group previously and the film composition as well as the properties of the a-C matrix were investigated using RBS, XPS, TEM and Raman spectroscopy (Gerhards *et al* 2003).

In addition to experimental characterization of MSIBD grown ta-C films, molecular dynamics simulations provide insight in the creation of ion tracks in ta-C and also in the formation of hillocks on the impact site of each ion (Schwen 2007, Schwen and Bringa 2007, Schwen *et al* 2012). The simulations reveal a sp^2 content of up to 86% in the track and >97% in the hillocks. According to theses MD simulations and experimental results, the hillock height increases linearly with the electronic energy loss of the ions.

The ta-C films used in this work were synthesized at the University of Göttingen by means of low energy MSIBD at room temperature. Heavily n-doped Si (0.005 Ω cm) was used as substrate material. Before film deposition the silicon surface was Ar^+ sputtered to remove the native oxide layer and to amorphize the surface in order to improve the contact of the ta-C film to the substrate. The ion source was charged with CO_2 gas and $^{12}C^+$ was deposited at 100 eV. The base pressure during deposition was 10^{-6} Pa. Due to mass separation, pure and hydrogen free films were produced. For doping of the ta-C films, Cu ions were provided to the ion source by evaporating $CuCl_2$. The Cu impurities were incorporated as 100 eV $^{63}C^+$ ions by rapid periodically switching the mass separation magnet from $^{12}C^+$ to $^{63}Cu^+$ and back. During the switching time the beam was electrostatically blocked to avoid contamination with ions of intermediate masses. Film growth and dopant concentration were controlled *in situ* via the deposited charge of the individual ion species onto the substrate. Usually, a total charge of 0.4 C was deposited, which corresponds to a ta-C film thickness of about 80 nm (calibrated by TEM analysis) on an area of about 200 mm^2. However, due to beam inhomogeneities the film thickness can slightly vary over the whole area. We estimate the uncertainty of the film thickness to be ±10%. The Cu concentration was determined directly after film growth by XPS analysis from the ratio of the C-1s and Cu-2p3/2 lines. The results are in agreement with previous RBS measurements (Gerhards *et al* 2003) showing that nearly all Cu is incorporated into the films. The uncertainty for the Cu concentration is estimated to be ±10%. Also immediately after deposition, the fraction of the sp^3-bonded carbon atoms in the film was determined via the position of the plasmon peak in electron energy loss measurements (Reinke *et al* 2004). According to these measurements the undoped and doped samples had similar sp^3 contents (>80%), except the 5 at.% Cu doped sample which had a sp^3 content which was about 10% lower.

The irradiation with U ions was performed at the GSI Helmholtz Centre in Darmstadt with initial beam energy of 2.2 GeV. To increase the energy loss of the ions, 49 μm thick aluminium foils were placed in front of the samples which degraded the beam energy to 1 GeV. When entering the sample surface, the ions had equilibrium charge state. The applied fluence was kept low (usually 4×10^9 ions cm^{-2}) in order to avoid track

Table 1. Parameters of ta-C samples doped with different Cu concentrations. The film thickness and Cu concentration were derived from the ion fluence controlled continuously during deposition, uncertainties are estimated to be ±10%. The undoped samples were used for AFM (*) and for macroscopic resistivity (**) measurements.

Cu concentration (at.%)	Film thickness (nm)	Irradiation fluence (10^9 ions cm^{-2})
0*	60	4
0**	80	40
0.5	65	4
1.0	65	4
2.0	65	4
5.0	45	4

overlapping. All irradiations were performed at room temperature and under normal beam incidence. The specification of the samples and irradiation conditions are summarized in table 1. The 60 nm thick undoped sample (0* in table 1) was investigated by AFM but showed an unsystematic behaviour in macroscopic resistivity measurements. We thus performed these measurements on a different sample (0** in table 1).

The conductivity and topography of the ion tracks were investigated by AFM measurements at the Harz University in Wernigerode using a XE-100 AFM (manufactured by PSIA Corp.) equipped with a conductive cantilever (BS-EM75) coated with Pt/Ir. To record current–voltage (*I*–*V*) curves of individual tracks, the AFM tip was brought in contact with the hillock at the ion impact site.

Macroscopic electrical measurements using a Keithley 237 SMU were performed in the temperature range between 15 and 390 K at the University of Göttingen. For the front contact, circular pads (diameter 0.6 mm) were deposited on the ta-C surface by thermal evaporation of a ∼10 nm thick layer of Cr followed by a ∼100 nm Au film. The highly-conducting Si substrate served as back contact. The back side of Si was contacted by silver paste with the current circuit. For the voltage measurement a third contact was attached to the front side of the Si substrate. This 'three-terminal' arrangement eliminates the resistance of the Si/silver paste contact. However, the resistances between the top pad and the ion track and between the ion track and Si remain.

3. Results and discussion

3.1. AFM measurements on single ion tracks at ambient temperature

Figure 1 shows typical AFM scans in a three-dimensional representation including topography images (left) and simultaneously recoded current maps (right). The two upper images refer to the undoped, the lower to a Cu-doped (1 at.%) sample. The topography images show surface hillocks of a few nm height attributed to the impact of individual ions (for a general review of ion-induced hillocks see e.g. Neumann 1999). Within the typical fluence uncertainties and inhomogeneities of 10% to 20%, the number of observed hillocks is in agreement with the number of ion impacts. Comparing the simultaneously recorded current and topography images, it is obvious that every impinging ion forms a conducting channel through the ta-C film.

The topography images (left) indicate that doping increases the surface roughness, and, to some surprise, decreases the mean hillock height. The current images (figure 1 right) reveal a clear improvement of the track currents with doping. For the undoped sample (upper right) the individual currents vary from track to track, whereas current peaks of the Cu-doped film (lower right) exhibit a much smaller height distribution and the average currents are significantly higher. Doping between 0.5 at.% and 2 at.% yields similar results. The 5 at.% sample is certainly over-doped, no tracks were found in the AFM measurement. This degradation is probably caused by the more relaxed structure of the higher-doped samples since a relaxed structure is less affected by the ion beam with the consequence that irradiation does not change the bonding character substantially.

The quantitative analysis (statistical distribution) of hillock heights and track currents is shown in figure 2. The average hillock height is maximum for the pristine film and for 0.5 at.% Cu doping and decreases for higher Cu concentrations. The track currents of doped films are significantly higher than for undoped films, but they show no clear dependence on doping concentration.

In table 2 the results of the AFM measurements are summarized. Hillock heights and currents I_{track} are the average values of at least 100 individual ion tracks recorded at a voltage of 0.3 V between AFM tip and the substrate. The given uncertainties correspond to the standard deviation of the arithmetic mean value.

3.2. Current measurement with macroscopic contact pads

The temperature dependence of the current through the sample was investigated with macroscopic contact pads. In the standard experiment, the contact covered an area of 0.28 mm^2 and connected approximately 10^7 ion

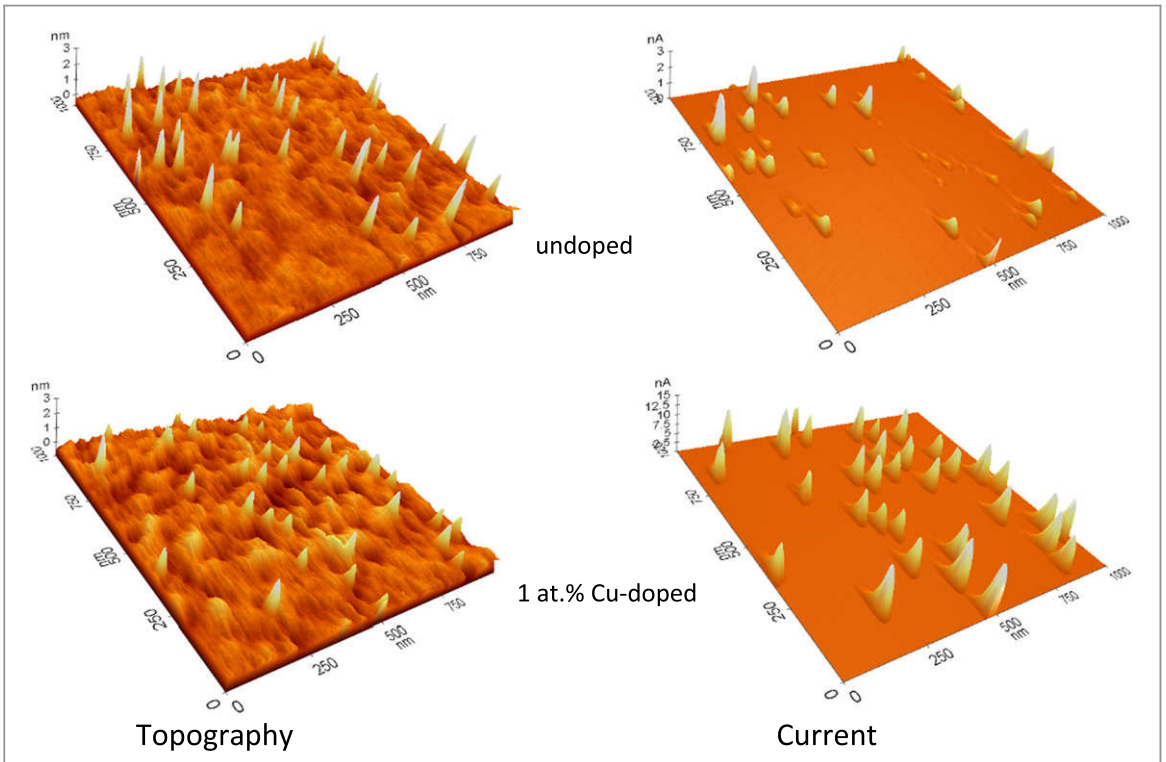

Figure 1. AFM images of undoped (top) and 1 at.% Cu-doped (bottom) ta-C films irradiated with 1 GeV U ions (nominal fluence 4×10^9 ions cm^{-2}) displaying surface topography (left) and simultaneously recorded current images (right). The current was measured between the AFM tip and the Si substrate at a bias voltage of 0.3 V. The shape of the peaks is mainly a result of the AFM tip shape.

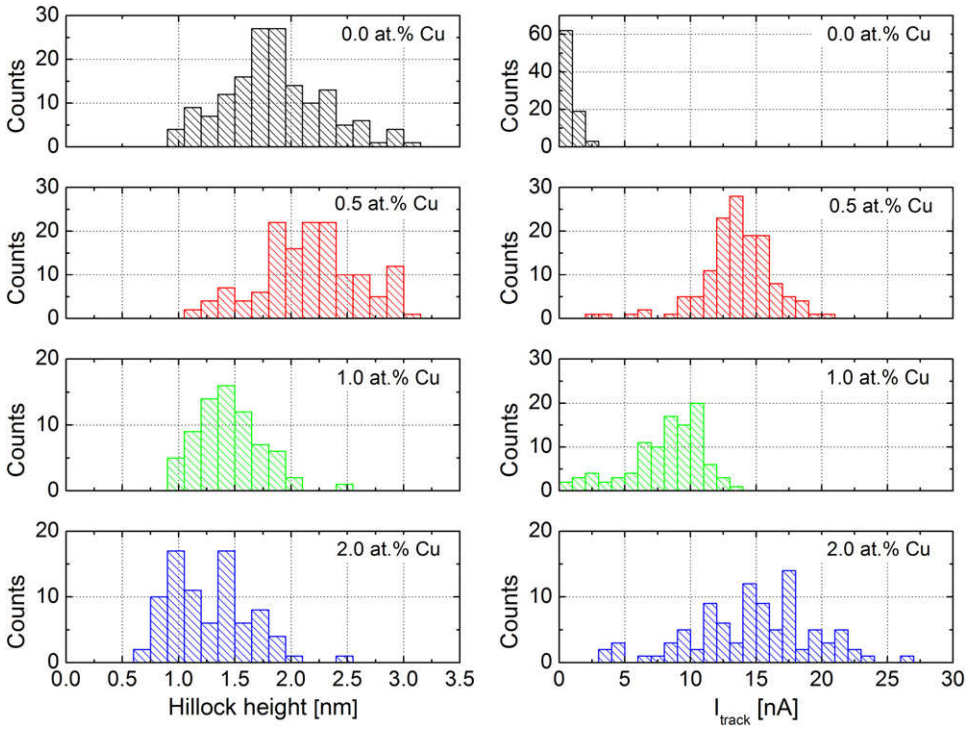

Figure 2. Distribution of hillock heights (left) and track currents I_{track} recorded with a bias voltage of 0.3 V at room temperature (right) for pure and Cu-doped ta-C samples (see also table 2).

Table 2. AFM characterization of pure and Cu-doped ta-C samples. Neither hillocks nor conducting tracks were detected for the 5 at.% Cu-doped sample.

Cu concentration (at.%)	Hillock height (nm)	Track current I_{track} at 0.3 V (nA)
0	2.17 ± 0.18	0.7 ± 0.08
0.5	2.20 ± 0.19	13.7 ± 0.21
1.0	1.36 ± 0.09	8.2 ± 0.23
2.0	1.17 ± 0.08	14.8 ± 0.48
5.0	—	—

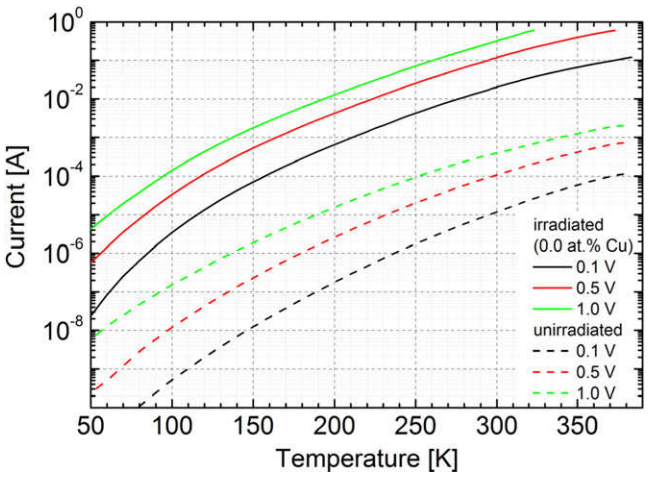

Figure 3. Comparison of an irradiated and an unirradiated pure ta-C sample. The current was measured with a 0.28 mm^2 contact pad at different applied external voltages as a function of temperature. The sample was irradiated with 1 GeV uranium ions to a nominal fluence of 4×10^{10} ions cm^{-2}.

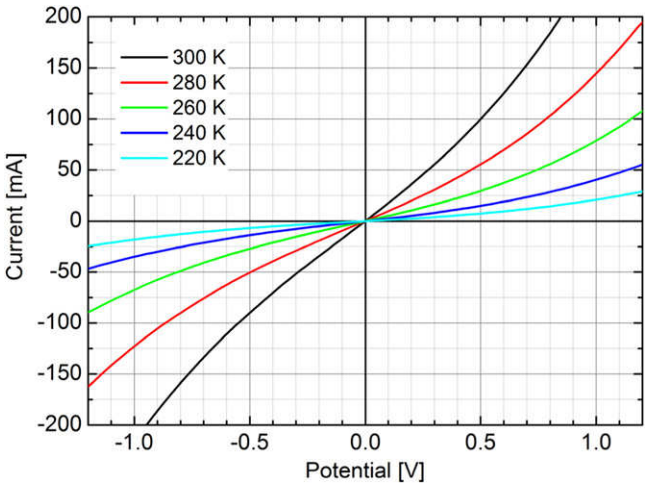

Figure 4. Current–voltage (*I–V*) characteristics measured with a macroscopic contact pad (0.6 mm Ø, averaging over about 10^7 ion tracks) at different temperatures for the 1 at.% Cu-doped sample.

tracks in parallel. The current was measured for different applied external voltages as a function of temperature. A typical result of these measurements is shown in figure 3.

Typical current–voltage (*I–V*) characteristics are displayed in figure 4. The currents are strongly temperature dependent and the *I–V* characteristics are bent, i.e., they do not follow Ohm's law.

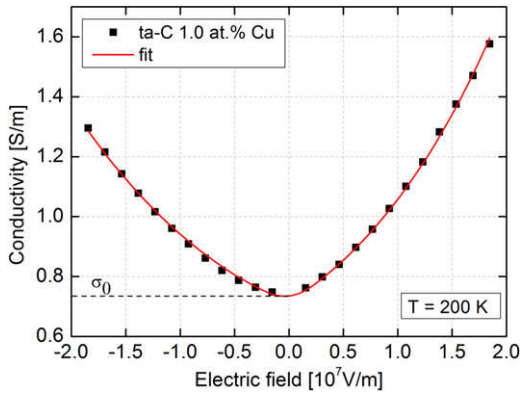

Figure 5. Conductivity of ion tracks in ta-C (doped with 1 at.% Cu) at 200 K as a function of applied electrical field $E = V/d$. The sample was irradiated with 1 GeV U ions to a fluence of 4×10^9 ions cm^{-2}. The solid line is a fit with the stretched exponential function and an asymmetry term (see section 3.4).

For the further presentation of the data and for the analysis we use reduced quantities in order to eliminate the specific geometries of the measurement and make details of the data more evident. The reduced quantities, conductivity σ and electrical field E, are defined as:

$$\sigma = \frac{I \cdot d}{V \cdot A} \text{ and } E = \frac{V}{d} . \tag{1}$$

Here I is the measured current, V the applied voltage and d the ta-C film thickness. The area A of the conducting path is specific for each arrangement: For the AFM measurements we used the area of a single track A_{track} which we calculate assuming a track diameter of 8 nm (Krauser *et al* 2003). For the macroscopic measurements the contact area (circular pad with 0.6 mm diameter) is the relevant quantity. For the matrix data the entire area is used. The track conductivity σ_{track} in the macroscopic measurements is calculated by the following formula:

$$\sigma_{track} = \frac{I_{irr} - I_{unirr}}{V} \cdot \frac{d}{A_{track} \cdot N_{track}} . \tag{2}$$

A_{track} is the cross sectional area of a single track (as above) and N_{track} is the number of tracks under the contact pad (derived from the track density measured by AFM). The area covered by ion tracks accounts only for about 1% of the total area. Thus some current is flowing also through the unirradiated parts of the sample under the contact. We have corrected for that by subtracting the current I_{unirr} measured on the matrix from the current I_{irr} measured on the irradiated sample (see equation (2)). Due to the large difference of track and matrix conductivity, this correction is very small, i.e., in the order of 1% or less. Only in the low-temperature region (below about 50 to 100 K) where a current offset is observed in some measurements, the correction becomes larger. We therefore consider the data below about 100 K as unreliable and did not include them in the quantitative analysis.

Figure 5 shows that the conductivity is field dependent, i.e., the current–voltage characteristics do not follow Ohm's law. However, the zero-field conductivity, obtained by an extrapolation from higher fields, is well defined. We used a phenomenological function for this extrapolation (for details see section 3.4).

The conductivity dependence on the electric field is asymmetric. The asymmetry, obtained by multiplying the fit function with the term $(1 + \text{const} \cdot E)$ amounts to 5.8% in the above case and is fairly constant (approximately 6%) for all samples and temperatures in the macroscopic measurements. In the AFM measurements slightly lower asymmetries were seen. We assume that the asymmetry is due to a Schottky barrier at the front contact or at the transition from ta-C to the substrate. This barrier adds a serial resistor in the measuring circuit and alters the conductivity attributed to the sample. The effect on the absolute conductivity values is in the order of 10%, the relative conductivity values are probably not much affected since the experimental asymmetry term is fairly independent of temperature and doping.

3.3. Zero-field conductivity σ_0

The zero-field conductivity σ_0 was obtained by extrapolating the values measured at finite fields to field zero. For an optimum extrapolation, all data were fitted by a stretched exponential function (equation (8)) with free parameters. The zero-field conductivity σ_0 as a function of temperature (reciprocal scale) is shown in figure 6.

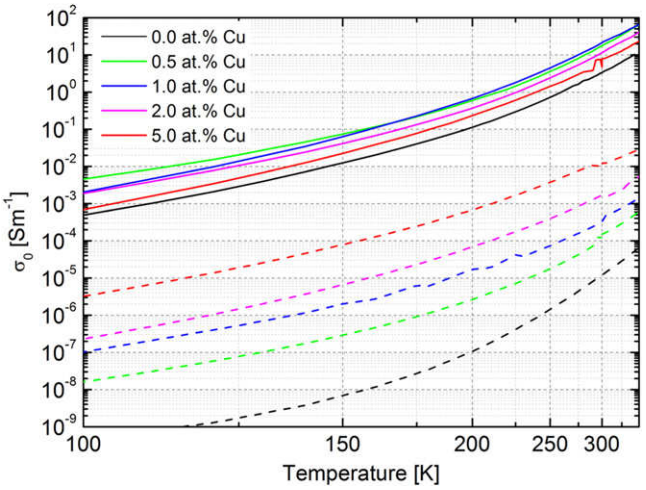

Figure 6. Zero-field conductivity σ_0 for different Cu-doping concentrations as a function of temperature (reciprocal scale) for ion tracks (solid lines) and ta-C matrix (dashed lines).

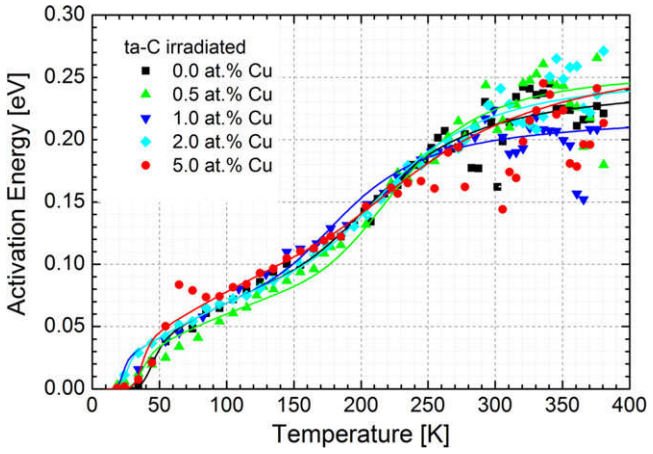

Figure 7. Effective activation energies E_{eff} for tracks in undoped and Cu-doped samples as a function of temperature. The solid lines are fits with a superposition of three processes: constant σ_0 at low temperatures, $T^{-1/4}$ dependence at intermediate temperature and a unique activation energy around room temperature (see text).

The shape of the temperature dependence is very similar in all cases but the absolute values differ by orders of magnitude.

For a thermally activated process the conductivity is given by:

$$\sigma_0 \propto \exp\left(-\frac{E_a}{k_B \cdot T}\right), \tag{3}$$

where E_a is the activation energy and k_BT the product of temperature and Boltzmann constant. A singly-activated thermal process does not describe our data because it would require a straight line in the log-scale of figure 6.

To see more clearly the change of the activation energy with temperature we calculated the slope of the curves in figure 6 and assigned it to effective activation energy E_{eff} by:

$$d\left(\ln \sigma_0\right)/d\left(1/T\right) = E_{\text{eff}}/k_B. \tag{4}$$

The results are presented in figure 7. The effective activation energies saturate around room temperature with values between 200 and 250 meV. We interpret this value as the barrier height for the transport in the ion tracks. For the matrix data the saturation energy (not shown here) is found to be slightly higher, the value lies in the region of 260 meV.

Figure 8 shows conductivity data (log-scale) as a function of $T^{-1/4}$. In the intermediate temperature region below RT the data are well represented by the $T^{-1/4}$ dependence (straight line) as predicted by Mott's variable-

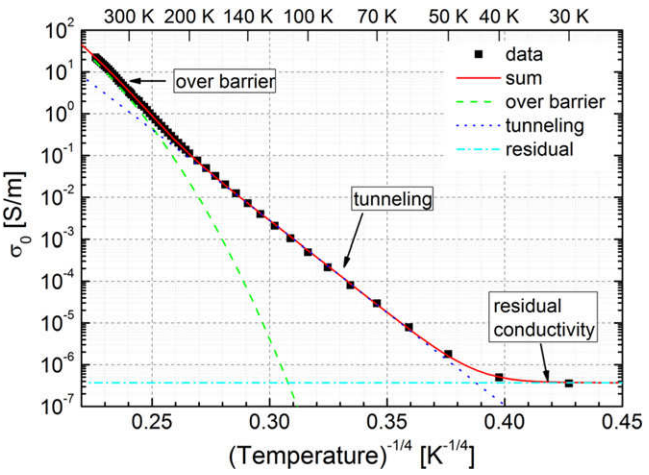

Figure 8. Logarithmic presentation of zero-field conductivity σ_0 versus $T^{-1/4}$ for ion tracks in pure ta-C. The high-temperature part (around room temperature) is interpreted as over-barrier hopping. In the intermediate temperatures region a straight-line behaviour indicates a tunnelling process (as in Mott's variable-range hopping model Mott 1968). The low-temperature residual conductivity is probably due to small shunt currents.

range hoping model (Mott 1968). We assign this part to a tunnelling process. Around room temperature a transport with unique activation energy takes over. We attribute this process to over-barrier hopping. The conductivity offset at very low temperatures is probably an experimental artefact since its value varies in a non-systematic way with the sample and setup conditions.

3.4. Field dependence

The dependence of the conductivity on the external electrical field is usually ascribed to a lowering of the transport activation energy E_a by the field, i.e.:

$$\sigma \propto \exp\left(-\frac{E_a - f(E)}{k_B \cdot T}\right) = \exp\left(-\frac{E_a}{k_B \cdot T}\right) \cdot \exp\left(\frac{f(E)}{k_B \cdot T}\right), \tag{5}$$

where $f(E)$ is a function of the electrical field E. This equation separates the zero-field conductivity and the field dependence.

The field dependence is often described by the Frenkel–Poole model (Frenkel 1938) which assumes that the transport occurs by lifting the electron to the conduction band. The external electrical field reduces the Coulomb attraction thereby lowering the activation energy for transport. The corresponding field dependence is given by:

$$\sigma = \sigma_0 \exp\left(\frac{f(E)}{k_B \cdot T}\right) = \sigma_0 \exp\left(\frac{\sqrt{b' \cdot E}}{k_B \cdot T}\right) \text{ with } b' = \frac{e^3}{\pi\varepsilon_0\varepsilon} \quad \text{(Frenkel−Poole model)}, \tag{6}$$

where e is the electrical charge and ε_0 and ε are the vacuum dielectric constant and its relative value in the material, respectively. The Frenkel–Poole model yields acceptable fits for the unirradiated ta-C samples around room temperature but the extracted ε value is largely unphysical and varies strongly with temperature.

The ion track data cannot be described by the Frenkel–Poole formula: the fitted ε values are much too large (in the order of 1000 times or more) and the functional dependence is close to being proportional to E rather than $\sqrt{E}$. We therefore analysed the data within a model derived by Pollak and Riess (1976). These authors apply a percolation approach to construct the conducting path. In this model the field dependence is given in the three-dimensional case by:

$$\sigma = \sigma_0 \exp\left(\frac{f(E)}{k_B \cdot T}\right) = \sigma_0 \exp\left(\frac{eEl}{k_B \cdot T}\right) \text{ with } l = 0.17 \cdot R \quad \text{(Pollak−Riess model)}, \tag{7}$$

where e is the electrical charge and R the hopping distance at low fields. The factor 0.17 is a special result of the percolation treatment by Pollak and Riess and accounts for the fact that the voltage drop per step is not E times the jump distance but is reduced due to directional and chemical potential effects.

Because of the uncertainty in the functional dependence, we chose a phenomenological approach of the form:

$$\sigma = \sigma_0 \exp\left((bE)^c\right), \tag{8}$$

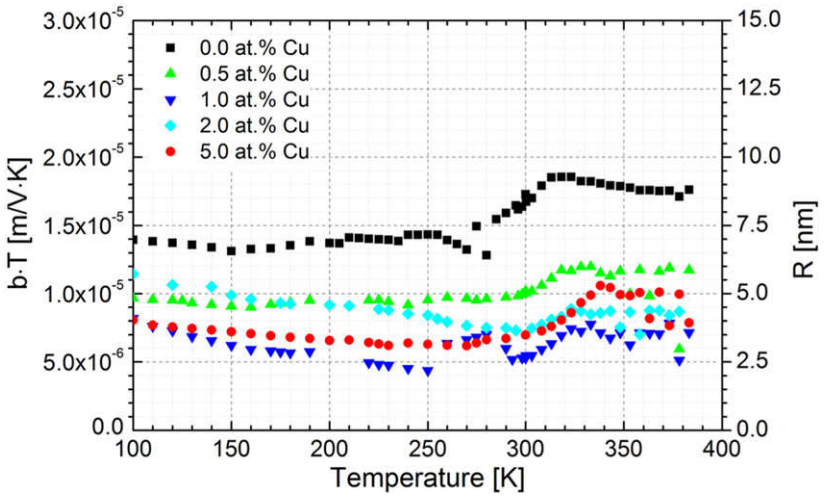

Figure 9. Bending parameter b multiplied by temperature T, for the track data as a function of temperature. The right scale gives the jump distance R deduced from $b \cdot T$ via the Pollak–Riess formula (equation (7)). The b-values were obtained by fitting the field dependence with a pure exponential function.

Table 3. Conductivity of ion tracks and ta-C matrix for pure and Cu-doped samples at room temperature. Track conductivities were obtained by AFM measurements on single tracks and by macroscopic measurements on track ensembles ($\sim 10^7$ tracks). Statistical errors within one measurement are small (% region) but the systematic errors due to normalization problems and sample inhomogeneities may be large (see text). The contrast data $\sigma_{track}/\sigma_{matrix}$ are deduced from macroscopic measurements.

Cu concentration (at.%)	Track conductivity σ_{track} (AFM) (S m^{-1})	Track conductivity σ_{track}(macro) (S m^{-1})	Matrix conductivity σ_{matrix} (S m^{-1})	Contrast $\sigma_{track}/\sigma_{matrix}$
0.0	2.61	3.0	1.0×10^{-5}	3.0×10^{5}
0.5	58.0	17.2	1.0×10^{-4}	2.0×10^{5}
1.0	35.6	23.5	3.0×10^{-4}	8.0×10^{4}
2.0	65.1	11.4	1.3×10^{-3}	8.0×10^{3}
5.0	—	4.7	1.0×10^{-2}	6.0×10^{2}

where σ_0 is the zero-field conductivity and b and c are adjustable parameters. Parameter b determines mainly the magnitude of the field dependence whereas parameter c reflects the shape of the dependence (see figure 5). The asymmetry (see figure 5) was taken into account by fitting the negative and positive field branch separately and averaging the fit parameters. In a first step we fitted all data with free parameters b and c. This yielded good fits and allowed a precise extrapolation to zero-field as mentioned above. However, we found that b and c are correlated in the fits leading to a large scatter of the individual values and making a comparison of data difficult. In order to describe the degree of bending by a single parameter we fixed the value of c to $c = 1$ for the track data.

Figure 9 displays data of the irradiated samples for the bending parameter b, multiplied by temperature T, and the jump distance R deduced from $b \cdot T$ via the Pollak–Riess formula (equation (7)). The product $b \cdot T$ and correspondingly the jump distance R are approximately constant for each sample; at least no clear tendency with temperature is seen. This implies that the bending parameter b increases with decreasing temperature as $1/T$ as expected if the activation energy for transport is reduced by the field (see equation (5)). We also notice that in the average the bending (deviation from Ohm's law) is smaller for the doped samples (coloured points) than for pure ta-C (black points). The doped samples have a higher conductivity, thus the bending decreases if the tracks are better conducting. Above 300 K the $b \cdot T$ values are systematically somewhat higher than in the lower temperature range. Note, however, that the setup was changed at around 300 K and instrumental effects cannot be excluded.

The matrix data (unirradiated samples) were reasonably well fitted with $\sqrt{E}$ dependence as predicted by the Frenkel–Poole model. The extracted ε values (not shown here) varied between about 20 and 200 and were larger for better conducting samples. They were also strongly temperature dependent. These large values and their variation with temperature and doping indicate that the Frenkel–Poole model is not well suited for the description of the data.

3.5. Doping dependence

The preceding data clearly show that Cu doping improves the electrical conduction of the ion tracks. The progress is twofold:

(i) Doping leads to tracks with a narrow conductivity distribution whereas the track conductivity scatters considerably in the undoped ta-C sample (see figures 1 and 2).

(ii) The overall conductivity of ion tracks increases by approximately an order of magnitude for doping with 0.5 at.% to 2 at.% Cu (see table 3). For 5 at.% Cu doping, the macroscopic measurements show a conductivity decrease, and no tracks could be found by means of AFM measurements.

The improvement of the conductivity along the percolation path may be due either directly to a bridging effect of the (conducting) dopant atom between bonds or indirectly to a catalytic effect which increases the concentration of (conducting) sp^2 bonds. The present data do not allow a final decision between these possibilities.

A significant result is that the hillock height decreases with increasing Cu concentration. For the 5 at.% Cu sample no hillocks could be found in AFM measurements (see table 2). The hillocks develop during the hot phase of the track formation process due to the expansion of the material in the ion track region and its outflow at the surface. Thus the lower height of the hillocks indicate that the density difference between track and matrix is less pronounced in the doped samples. It turns out that the incorporation of only a few atomic percent Cu impurities can lead to drastic structure changes in the film preventing hillock and track formation. This includes the reduction of compressive stress and an increased sp^2 fraction. The latter explains the high matrix conductivity of the Cu-doped unirradiated sample (see table 3). Gerhards *et al* reported a continuous decrease of the sp^3 fraction with increasing Cu incorporated in their ta-C films (Gerhards *et al* 2003). It should be pointed out that we have so far found only extremely poor conducting tracks together with almost undetectable hillocks in plasma deposited a-C:H films. Such films are known to be more graphitic and less stressed.

A disadvantage of Cu doping is that it decreases the insulating behaviour of the matrix by orders of magnitude. Moreover, the conductivity of the doped matrix increases stronger than the conductivity of the tracks (see figure 6 and table 3 as well as (Ronning *et al* 1995) yielding a decrease of current contrast between track and matrix (table 3). Whether the improvement gained by doping outweighs the disadvantage of lower contrast may depend on the specific situation.

Table 3 shows the track conductivities measured by two different methods: By AFM on single tracks and subsequent averaging over about 100 tracks and by macroscopic contact pads averaging over about 10^7 tracks within one measurement. The general trend of the data obtained by these two approaches is similar but quantitative agreement is not complete. This is not surprising since each of the methods has shortcomings. In the AFM measurements a very small area (typically 1 μm^2) is investigated. Thus local sample inhomogeneity may influence the results. In macroscopic measurements good electrical contacts are crucial. If not all tracks are contacted or if the contact area deviates from the nominal area quite different absolute values can be obtained. In view of these difficulties the agreement within the two methods is satisfactory.

3.6. Barrier model

The material modified along the ion tracks is assumed to be rather inhomogeneous. Areas of mainly planar sp^2 coordination are separated by regions dominated by tetragonal sp^3 bonding (see e.g. Dasgupta *et al* 1991, Maiken and Taborek 2000, Khan *et al* 2001). The electrons move along a percolation path in better conducting sp^2 regions but also have to pass through more insulating barriers dominated by sp^3 bonds. Thus sp^3 regions constitute barriers for the electrical current and determine to a large degree the resistivity of the track. The electron can either tunnel through the barrier or jump over it. The tunnelling process leads to the observed $T^{-1/4}$ temperature dependence at lower temperatures. The over-barrier hoping corresponds to an activated process with fixed activation energy as observed around room temperature and above. The barrier height, derived from the present experiment, is in the order of 200 to 250 meV.

The width of the barrier is a critical parameter for the tunnelling matrix element. The observed jump range of about 5 nm (see figure 9) is certainly too large to correspond to the barrier width if the barrier height is 200 meV or more. A rough estimate of the width can be obtained by the following considerations: at about 200 K we see a transition from tunnelling to over-barrier hopping (figure 8) indicating that the transition rates for tunnelling and over-barrier hopping are about equal. We thus equate the two rates at this temperature, i.e., $\exp(-2R/\alpha_0) \cdot \exp(-E_{\mathrm{eff}}/kT) = \exp(-E_a/kT)$, where α_0 is the penetration depth, R the tunnelling distance, k the Boltzmann constant and T the temperature. With $E_{\mathrm{eff}} = 100$ meV at 200 K and $E_a = 220$ meV (see figure 7) we obtain $\exp(-2\,R/\alpha_0) \approx 10^{-3}$. The penetration depth α_0 (sometimes also called Bohr radius) is not known in the present case. Maiken and Taborek assumed α_0 values between 0.1 and 1 nm (Maiken and Taborek 2000) in their conductivity studies of amorphous carbon. With these values for α_0, the tunnelling probability of 10^{-3} is obtained for $R = 0.35$ nm and $R = 3.5$ nm, respectively. Another scale for the penetration depth (Bohr radius) might be the interatomic distance in amorphous carbon (about 0.15 nm). With twice the atomic distance for α_0, the tunnelling probability of 10^{-3} is obtained for a tunnelling distance of about 1 nm. These estimates are of

course not a real determination of the barrier width but they indicate that the tunnelling distance is smaller than the experimental jump range of about 5 nm.

We thus suggest that the width of the barrier is only a few atomic distances wide. After traversing the barrier, the electron moves in a fairly well-conducting region before it reaches the next barrier. The jump distance is composed of the width of the barrier and the path of the electron in the well-conducting region.

A crucial role for the track conductivity plays the sp^2/sp^3 ratio. A larger sp^2 content leads to an increase of the density of states near the Fermi energy. But this is not the main cause for the better conductance. The main change concerns the density of low-energy barriers. If this density is larger, more electrons can find a percolation path with low barriers. In poorly-conducting materials many electrons, even if they are in sp^2-like bonds, are immobilized since they are surrounded by high-barrier sp^3-like bonds.

The well-conducting and poorly-conducting tracks show another distinct difference: The bending parameter b of the field dependence decreases with increasing conductivity (see figure 9), i.e., the tracks become more ohmic. A smaller bending parameter means that the potential reduction per jump decreases indicating that the number of jumps necessary to reach the electrode goes up. This indicates that the material becomes more homogeneous and that the dominance of the barriers which govern the poorly-conducting tracks goes down.

4. Conclusion

The temperature and field dependence measurements presented in this paper permit a deeper understanding of the mechanism of the electrical conduction of ion tracks in ta-C. Important information is obtained by separating the field dependence from the zero-field conductivity allowing an independent discussion of these two phenomena. The data are interpreted in the so-called 'barrier model' where we assume that the electrons move mainly in the rather-well conducting sp^2 region but encounter barriers of sp^3-like bonds along their path that have to be overcome. Based on temperature dependent conductivity measurements we conclude:

(i) Around room temperature and above an activated process with a fixed activation energy (about 220–260 meV) exists. We suggest that this process corresponds to over-barrier hopping and that the barrier height is given by the energy position of the excited state in the barrier region.

(ii) At lower temperatures the famous $T^{-1/4}$ law is observed indicating a tunnelling process through a barrier. We suggest that the width of the barrier is only a few atomic distances wide, i.e., an electron tunnels through a few sp^3-like bonds before it reaches the next well-conducting sp^2-like region. The jump range comprises the short tunnelling distance through the barrier and the longer path length in the sp^2-like area.

(iii) Cu-doping in the concentration range of about 1 at.% leads to an improvement of the track conductivity by approximately one order of magnitude. However, at the same time, the matrix conductivity increases very strongly making the advantage of doping questionable.

Conducting tracks in a highly insulating ta-C matrix represent interesting nanostructures for applications in future nanodevices (see e.g. Weidinger 2004, Krauser *et al* 2008, 2012, Gehrke *et al* 2010). Given by the large range of swift heavy ions, rather complex nano-systems are possible. Irradiating e.g. a multilayered system interrupted by thin insulating layers may allow the realization of nanodots with conducting tracks as self-aligned contact leads on both sides.

Acknowledgments

Financial support for this work was provided by the DFG (HO1125/21-1) and (KR 3298/2-1). We acknowledge support by the Open Access Publication Funds of the Göttingen University.

References

Christiansen S, Albrecht M, Frank G, Strunk H P, Ronning C, Hofsäss H and Recknagel E 1998 Carbon transport in Si(001) and nucleation of diamond-like carbon layers during mass selected ion beam deposition *Diam. Relat. Mater.* **7** 15

Dasgupta D, Demichelis F and Tagliaferro A 1991 Electrical conductivity of amorphous carbon and amorphous hydrogentated carbon *Phil. Mag.* B **63** 1255

Frenkel J 1938 On pre-breakdown phenomena in insulators and electronic semiconductors *Phys. Rev.* **54** 647

Gehrke H-G 2008 *Diploma Thesis* II. Institute of Physics, University Göttingen

Gehrke H-G 2013 *Doctoral Thesis* II. Institute of Physics, University Göttingen

Gehrke H-G, Nix A-K, Hofsäss H, Krauser J, Trautmann C and Weidinger A 2010 Self-aligned nanostructures created by swift heavy ion irradiation *J. Appl. Phys.* **107** 094305
Gerhards I, Ronning C, Hofsäss H, Seibt M and Gibhardt H 2003 Ion beam synthesis of diamond-like carbon thin films containing copper nanocrystals *J. Appl. Phys.* **93** 1203
Hofsäss H, Binder H, Klumpp T and Recknagel E 1993 Doping and growth of diamond-like carbon films by ion beam deposition *Diam. Relat. Mater.* **3** 137
Hofsäss H, Feldermann H, Merk R, Sebastian M and Ronning C 1998 Cylindrical spike model for the formation of diamondlike thin films by ion deposition *Appl. Phys.* A **66** 153
Hofsäss H, Zhang K and Zutz H 2009 Nanostructured carbide surfaces prepared by surfactant sputtering *Nucl. Instrum. Methods* B **267** 1398
Khan R U A, Carey J D, Silva S R P, Jones B J and Barklie R C 2001 Electron delocalization in amorphous carbon by ion implantation *Phys. Rev.* B **63** 1212011
Koskinen J 1988 Abrasive wear resistance of ion-deposited hard-carbon films as a function of deposition energy *J. Appl. Phys.* **63** 2094
Krauser J, Gehrke H-G, Hofsäss H, Trautmann C and Weidinger A 2013 Conductive tracks of 30-MeV C_{60} clusters in doped and undoped tetrahedral amorphous carbon *Nucl. Instrum. Methods Phys. Res.* B **307** 265
Krauser J, Nix A-K, Gehrke H-G, Hofsäss H, Trautmann C and Weidinger A 2012 Conductivity enhancement of ion tracks in tetrahedral amorphous carbon by doping with N, B, Cu and Fe *Nucl. Instrum. Methods Phys. Res.* B **272** 280
Krauser J, Nix A-K, Gehrke H-G, Hofsäss H, Trautmann C and Weidinger A 2011 Highly conductive ion tracks in tetrahedral amorphous carbon by irradiation with 30 MeV C_{60} projectiles *New J. Phys.* **13** 083023
Krauser J, Nix A-K, Gehrke H-G, Hofsäss H, Trautmann C, Weidinger A, Wünsch F and Bruns J 2008 Ion track technology and graphitic nanowires in diamondlike carbon *J. Vac. Sci. Technol.* B **26** 2468
Krauser J and Weidinger A 2012 Conducting ion tracks in tetrahedral amorphous carbon: fundamentals and perspectives for applications *Dekker Encyclopedia of Nanoscience and Technology* 2nd edn ed S E Lyshevski (Boca Raton, FL: CRC Press)
Krauser J, Zollondz H, Weidinger A and Trautmann C 2003 Conductivity of nanometer-sized ion tracks in diamond-like carbon films *J. Appl. Phys.* **94** 1959
Kulik J, Lempert G D, Grossman J, Marton D, Rabalais J W and Lifshitz Y 1995 *Phys. Rev.* B **52** 15812
Lifshitz Y 1999 Diamond-like carbon—present status *Diam. Relat. Mater.* **8** 1659
Lifshitz Y, Lempert G D and Grossman E 1994 Substantiation of subplantation model for diamondlike film growth by atomic force microscopy *Phys. Rev. Lett.* **72** 2753
Maiken E B and Taborek P 2000 Amorphous carbon films deposited from carbon ions extracted from a discharge in fullerene vapor *J. Appl. Phys.* **87** 4223
Moseler M, Gumbsch P, Casiraghi C, Ferrari A C and Robertson J 2005 Materials science: the ultrasmoothness of diamond-like carbon surfaces *Science* **309** 1545
Mott N F 1968 Conduction in glasses containing transition metal ions *J. Non-Cryst. Solids* **1** 1
Neumann R 1999 Scanning probe microscopy of ion-irradiated materials *Nucl. Instrum. Methods Phys. Res.* B **151** 42
Neuville S 2014 *QScience Connect* **2014** 8
Nix A-K 2010 *Doctoral Thesis* II. Institute of Physics, University Göttingen
Nix A-K, Schwen D, Ronning C, Krauser J, Trautmann C and Hofsäss H 2007 Electronic properties of graphite-like ion tracks in insulating tetrahedral amorphous carbon *Rev. Adv. Mater. Sci.* **15** 192
Pollak M and Riess I 1976 A percolation treatment of high-field hopping transport *J. Phys. C: Solid State Phys.* **9** 2339
Reinke P, Garnier M G and Oelhafen P 2004 *In situ* photoelectron spectroscopy analysis of tetrahedral amorphous carbon films *J. Electron Spectrosc. Relat. Phenom.* **136** 239
Robertson J 2002 Diamond-like amorphous carbon *Mater. Sci. Eng.* R **37** 129
Ronning C 2003 Ion-beam synthesis and growth mechanism of diamond-like materials *Appl. Phys.* A **77** 39
Ronnig C, Dreher E, Thiele J U, Oelhafen P and Hofsäss H 1997 Electronic and atomic structure of undoped and doped ta-C films *Diam. Relat. Mater.* **6** 830
Ronning C, Griesmeier U, Gross M, Hofsäss H, Downing R G and Lamaze G P 1995 Conduction processes in boron- and nitrogen-doped diamond-like carbon films prepared by mass-separated ion beam deposition *Diam. Relat. Mater.* **4** 666
Ronning C and Hofsäss H 1995 *Diamond Materials I V Proc. 4th Int. Symp.*ed K V Ravi and J P Dismukes (Pennington: The Electrochemical Society) p 359
Schwen D 2007 Structural and electronic properties of swift heavy ion tracks in amorphous carbon *Doctoral Thesis* II. Institute of Physics, University Göttingen online at: (http://webdoc.sub.gwdg.de/diss/2007/schwen/schwen.pdf)
Schwen D, Bringa E, Krauser J, Weidinger A, Trautmann C and Hofsäss H 2012 Nano-hillock formation in diamond-like carbon induced by swift heavy projectiles in the electronic stopping regime: experiments and atomistic simulations *Appl. Phys. Lett.* **101** 113115
Schwen D and Bringa E M 2007 Simulation of ion tracks in diamond and graphite *Nucl. Instrum. Methods Phys. Res.* B **256** 187
Takahiro K, Zhang K, Rotter F, Schwen D, Ronning C, Hofsäss H and Krauser J 2007 Morphological change of carbon surfaces by sputter erosion *Nucl. Instrum. Methods* B **256** 378
VDI 2840 2005 Carbon films *VDI Richtlinien* Verein Deutscher Ingenieure: available at (http://vdi.de/uploads/tx_vdirili/pdf/9656068.pdf) (accessed 29 November 2013)
Waiblinger M, Sommerhalter C, Pietzak B, Krauser J, Mertesacker B, Lux Steiner M C, Klaumünzer S, Weidinger A, Ronning C and Hofsäss H 1999 Electrically conducting ion tracks in diamond-like carbon films for field emission *Appl. Phys.* A **69** 239
Weidinger A 2004 Ion tracks—a new route to nanotechnology *Europhys. News* **35** 152
Zollondz J-H, Schwen D, Nix A-K, Trautmann C, Berthold J, Krauser J and Hofsäss H 2006 Conductive nanoscopic ion tracks in diamond-like carbon *Mater. Sci. Eng.* C **26** 1171